Available online at www.sciencedirect.com
SCIENCE DIRECT®
PERGAMON
International Journal of Heat and Mass Transfer 46 (2003) 4381–4391
International Journal of HEAT and MASS TRANSFER
www.elsevier.com/locate/ijhmt

# Dendritic heat convection on a disc

W. Wechsatol [a], S. Lorente [b], A. Bejan [a,*]

[a] Department of Mechanical Engineering and Materials Science, Duke University, Box 90300, Durham, NC 27708-0300, USA
[b] Department of Civil Engineering, National Institute of Applied Sciences (INSA), 135 Avenue de Rangueil, Toulouse 31077, France

Received 23 December 2002; received in revised form 10 June 2003

**Abstract**

In this paper we develop the optimal tree-shaped flow paths for cooling a disc-shaped body by convection. Heat is generated uniformly over the disc area. The coolant enters through the center of the disc, and exits through ports positioned equidistantly along the perimeter. The unknown is the flow architecture. The constraints are the disc size and the total volume occupied by the ducts. It is assumed that the ducts are narrow enough so that the flow is hydrodynamically and thermally fully developed. The ultimate goal is to determine flow architectures that reach *simultaneously* two objectives: (i) minimal global fluid flow resistance (or pumping power), and (ii) minimal global thermal resistance. When the architecture is optimized for (i), the result is a dendritic structure in which every geometric feature is uniquely determined. The corresponding thermal resistance decreases as the total mass flow rate and the pumping power increase. When the objective is (ii), the optimal architecture has radial ducts, not dendrites. The corresponding fluid-flow resistance increases as the flow rate increases and the global thermal resistance decreases. Put together, these geometric results show that methods (i) and (ii) lead to nearly the same combined performance (thermal and fluid). Examined more closely, the dendrites produced by method (i) perform progressively better as the length scales become smaller. Optimized increasing complexity is the route to high thermal and fluid-flow performance in the limit of decreasing scales.
© 2003 Elsevier Ltd. All rights reserved.

*Keywords:* Constructal theory; Dendritic; Tree networks; Fractal; Optimization; Small scales; Topology; Constructal design; Miniaturization

## 1. Objective

Constructal theory [1] recommends the use of a hierarchical tree-shaped (dendritic) path as the geometric form that maximizes the access of a stream between one point (source, or sink) and an infinity of points (volume, or area). Dendritic flow architectures were first reported for the cooling of electronics [2], where they were used for optimizing the insertion of high-conductivity blades and needles into the heat-generating packages. Trees for heat conduction and convection, fin assemblies, fluid flow, traffic, economics and business were optimized based on constructal theory, and are reviewed in [1]. In particular, trees for convection were analyzed by Bejan and Errera [3], Bejan et al. [4], Pence [5], Wechsatol et al. [6–8], Chen and Cheng [9] and Lorente et al. [10]. Trees for conduction (high-conductivity inserts) on a disc were optimized based on constructal theory by Rocha et al. [11], and based on numerical evolutionary algorithms by Xia et al. [12]. The interest in constructal flow architectures is spreading to other sectors of the field of heat and mass transfer, as illustrated by recent papers on the hierarchical geometric structures of boiling [1,13,14] (an idea continued in [15]) and heat exchangers and mass exchangers [16–18]. Important applications are also found in civil engineering and urban design [19].

In this paper we consider the fundamentals of optimizing geometry when the objective is the cooling by convection of a disc-shaped body that generates heat

* Corresponding author. Tel.: +1-919-660-5309; fax: +1-919-660-8963.
*E-mail address:* dalford@duke.edu (A. Bejan).

0017-9310/$ - see front matter © 2003 Elsevier Ltd. All rights reserved.
doi:10.1016/S0017-9310(03)00295-3

**Nomenclature**

| | |
|---|---|
| $c_p$ | specific heat at constant pressure, J kg$^{-1}$ K$^{-1}$ |
| $d_0$ | spacing between outlets on the disc perimeter, m |
| $D$ | duct diameter, or thickness of projected duct image, m |
| $f$ | dimensionless flow resistance, Eq. (17) |
| $j$ | pairing level |
| $k$ | thermal conductivity, W m$^{-1}$ K$^{-1}$ |
| $L_{0,1,2}$ | duct lengths, m |
| $\dot{m}$ | total mass flow rate, kg s$^{-1}$ |
| $\dot{m}''$ | mass flow rate per unit area, kg s$^{-1}$ m$^{-2}$ |
| $\dot{m}_0$ | mass flow rate through one central duct, kg s$^{-1}$ |
| $M$ | dimensionless mass flow rate, Eq. (7) |
| $n_p$ | number of outlets on the disc perimeter |
| $n_0$ | number of central ducts |
| $Nu$ | Nusselt number |
| $p$ | wetted duct perimeter, m |
| $p$ | construct level |
| $\widehat{P}$ | overall pressure drop, Eq. (19) |
| $q$ | total heat current, W |
| $q''$ | heat generation rate per unit area, W m$^{-2}$ |
| $r$ | radial position, m |
| $R$ | disc radius, m |
| $t$ | disc thickness, m |
| $T_f$ | fluid bulk temperature at the duct outlet, K |
| $T_m$ | maximum (hot spot) temperature, K |
| $T_w$ | wall temperature, K |
| $T_0$ | inlet temperature, K |
| $\widetilde{T}_m$ | dimensionless global thermal resistance, Eq. (5) |
| $U_0$ | mean fluid velocity, m s$^{-1}$ |
| $V$ | total duct volume, m$^3$ |
| $\dot{W}$ | pumping power, W |
| $x_1$ | radial distance between the first and second pairing levels, m |

*Greek symbols*

| | |
|---|---|
| $\Delta P$ | pressure drop, Pa |
| $\theta$ | angular coordinate, rad, Eq. (9) |
| $\mu$ | viscosity, kg s$^{-1}$ m$^{-1}$ |
| $v$ | kinematic viscosity, m$^2$ s$^{-1}$ |
| $\phi$ | projected area fraction occupied by the ducts, Eq. (1) |

*Superscripts*

| | |
|---|---|
| $\tilde{}$ | dimensionless variables, Eqs. (9) and (14) |
| $\hat{}$ | dimensionless variables, Eq. (18) |

volumetrically. The cooling effect is provided by a single stream of single-phase fluid, which enters the disc through its center, and flows toward the periphery. The objective is to find the flow patterns that minimize *at the same time* the hot-spot temperature of the solid, and the flow resistance encountered by the coolant.

For simplicity, we assume that the disc is sufficiently thin so that it can be modeled as a disc with uniform rate of heat generation per unit area ($q''$). The disc radius is $R$, and the fluid mass flow rate is $\dot{m}$. The heat is generated at every point in the solid material of thermal conductivity $k$. It is then conducted through the solid to the nearest flow channel, and, later, it is convected by the stream that flows through the channel.

The present study has three parts. In the first, we analyze the heat-transfer performance of tree-shaped flows that have been optimized for minimal flow resistance, or minimal pumping power. The second part of this study is devoted to the pure heat transfer problem of determining the flow patterns that minimize the global thermal resistance of the system. We also determine the corresponding fluid mechanics performance (pressure drop, pumping power) of the heat-transfer optimized cooling scheme. In the concluding part of the study, we consider the combined fluid-flow and heat-transfer optimization of the flow architecture. An important issue is whether the performance of the designs optimized in the first phase of this work is much different than the performance of the structures optimized in the second phase. Furthermore, is it necessary to optimize the flow structure for minimum thermal resistance and minimum flow resistance at the same time? Are the flow-optimized tree networks nearly optimal from a heat transfer standpoint?

Unlike in studies of thermodynamic optimization (e.g., [20–22]), in which the search is for a unique balance (for minimal irreversibility) between heat-transfer performance and fluid-flow performance, here we seek designs (architectures, configurations) in which both figures of merit are as high as possible. On a graph of thermal resistance versus fluid flow resistance (Fig. 1), we want the optimized flow architecture to be represented by a curve that is situated as close as possible to the origin. There is one curve for each flow architecture, as shown by the porous heat exchanger structures tested in [23]. The main features of these tests are illustrated qualitatively in Fig. 1. In forced convection configurations, the thermal resistance decreases as the pumping power increases. To determine the performance curve for each flow architecture is the objective of the analysis and optimization reported in this paper.

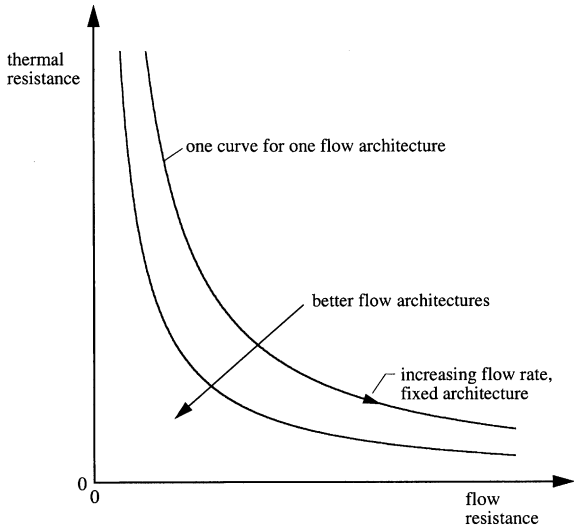


Fig. 1. Search for flow architectures with low thermal resistance and low fluid-flow resistance.

## 2. Radial flow pattern without branches

To develop the numerical model and nomenclature, consider the simplest design (Fig. 2): the coolant enters through the center of the disc, and flows along $n_0$ radial ducts. The mass flow rate through each duct is $\dot{m}_0 = \dot{m}/n_0$. When $n_0$ is of order 10 or greater, a sector that has one duct as centerline can be approximated by an isosceles triangle of base $2\pi R/n_0$ and height $R$. This triangular model is shown in the lower part of Fig. 2. In order to determine the global thermo-fluid performance of the disc-shaped system, it is sufficient to describe the flow of heat and fluid in one sector. It is assumed that the space occupied by the duct is a small fraction of the entire space,

$$\phi = \frac{n_0 DR}{\pi R^2} \ll 1 \tag{1}$$

Here $D$ is the thickness of the duct image projected on the disc area. The duct geometric aspect ratio is $D/R = \pi\phi/n_0$. The approximation (1) permits an analysis in which the ducts are treated as lines drawn on the disc. This limits the validity domain of the analysis, but justifies the calculation of pressure drops based on the long and thin duct sections, by neglecting the losses at junctions.

If $q$ is the total heat current generated by the disc, then the heat generation rate per unit area is $q'' = q/(\pi R^2)$. The effect of $q''$ is to raise all the temperatures above the lowest temperature ($T_0$), which belongs to the coolant inlet. The highest temperature ($T_m$) occurs in the two peripheral corners of the sector. The overall temperature difference that drives the heat transfer process is $T_m - T_0$. The overall thermal resistance of the disc is

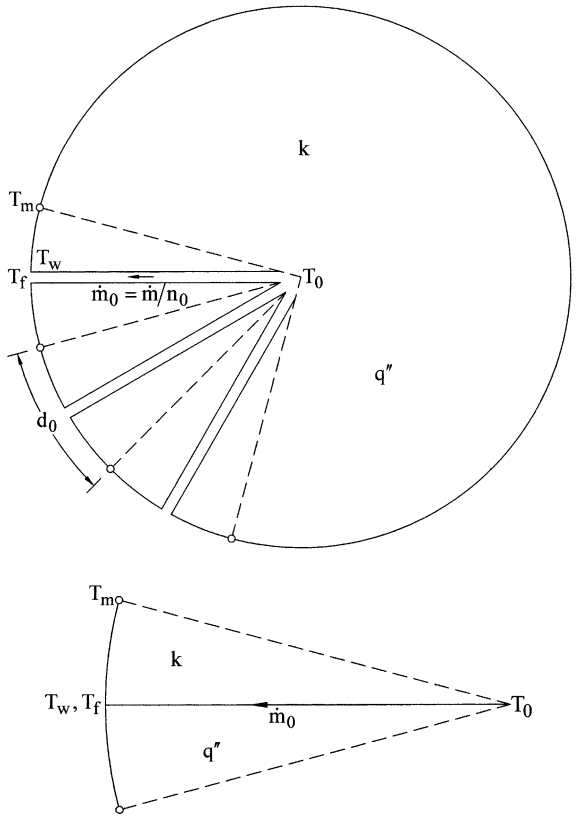


Fig. 2. Flow pattern with radial ducts, and isosceles triangle approximation of the sector associated with one duct.

$(T_m - T_0)/q$, which will be nondimensionalized later in Eq. (5).

We evaluate the thermal resistance by noting that when the sector is slender the conduction heat flux through the solid material of thermal conductivity $k$ proceeds in the direction perpendicular to the duct. The overall temperature difference $T_m - T_0$ is the sum of three contributions,

$$T_f - T_0 = \frac{\pi q'' R^2}{n_0 \dot{m}_0 c_p} \tag{2}$$

$$T_w - T_f = \frac{\pi q'' RD}{n_0 p k_f Nu} \tag{3}$$

$$T_m - T_w = \frac{\pi^2 R^2 q''}{2 n_0^2 k t} \tag{4}$$

where $T_f$, $T_w$, $t$, $k_f$ and $Nu$ are the fluid bulk temperature at the duct outlet, the duct wall temperature at the outlet, the disc thickness, the fluid thermal conductivity, and the Nusselt number based on $D$. Eq. (2) is the first law of thermodynamics applied to one sector. Eq. (3) is the statement that the heat current that arrives in the angular direction at the wall end of the duct, $q''\pi R/n_0$, is

the same as the heat current that flows from the wall to the fluid in the plane of the outlet, $hp(T_w - T_f)$, where $h$ and $p$ are the heat transfer coefficient and the wetted perimeter of the duct cross-section. We also used the Nusselt number definition $Nu = hD/k_f$, with the observation that for fully developed laminar flow Nu is a constant with a value between 1 and 10.

Eq. (4) is obtained from the temperature distribution along the perimeter of length $d_0/2 = 2\pi R/(2n_0)$, from $T_m$ to $T_w$. The analysis is described in [1] and [2]. In brief, because the solid generates heat at every point, the temperature distribution along the perimeter is parabolic, with zero temperature gradient at $T_m$, and the largest temperature gradient at $T_w$. The parabolic shape is such that the temperature gradient at $T_w$ is $4(T_m - T_w)/d_0$, i.e., twice the gradient based on the temperature difference separated by $d_0/2$. The heat flux that arrives at $T_w$, namely $kt[4(T_m - T_w)/d_0]$, is equal to the heat generation rate integrated along $d_0/2$, namely $(d_0/2)q''$. From this equality follows Eq. (4).

By adding Eqs. (2)–(4), and nondimensionalizing the sum as the overall thermal resistance of the disc,

$$\tilde{T}_m = \frac{T_m - T_0}{q/(kt)} \tag{5}$$

we obtain the expression

$$\tilde{T}_m = \frac{1}{M} + \frac{\pi\phi kt}{n_0^2 k_f p Nu} + \frac{\pi}{2n_0^2} \tag{6}$$

The number $M$ is a dimensionless mass flow rate,

$$M = \frac{\dot{m}c_p}{kt} \tag{7}$$

Alternatively, by using the heat-transfer-units concept of heat exchanger design, $M^{-1}$ may be regarded as the "number of conductive heat transfer units".

The three terms of $\tilde{T}_m$ represent, in order, (i) the radial temperature increase experienced by the coolant, (ii) the temperature difference between the duct wall and the fluid, and (iii) the maximum temperature difference across the heat-generating solid. The ratio between terms (ii) and (iii) is $2\phi kt/(Nuk_f p)$, in which $2/Nu$ is a number of order 1. This means that the second term is negligible in the limit of thin ducts, so thin that the projected area fraction $\phi$ is smaller than $k_f p/(kt)$. The following numerical work on radial ducts and more complicated configurations is based on the assumption that $\phi < k_f p/(kt)$, such that the wall-fluid thermal resistance is negligible.

The solid curves in Fig. 3 show the behavior of $\tilde{T}_m$ when the second term of Eq. (6) is neglected. The thermal resistance drops when the flow rate ($M$) increases. This trend matches the behavior anticipated in Fig. 1, because along with the increase in flow rate comes an increase in pumping power. The thermal resistance also

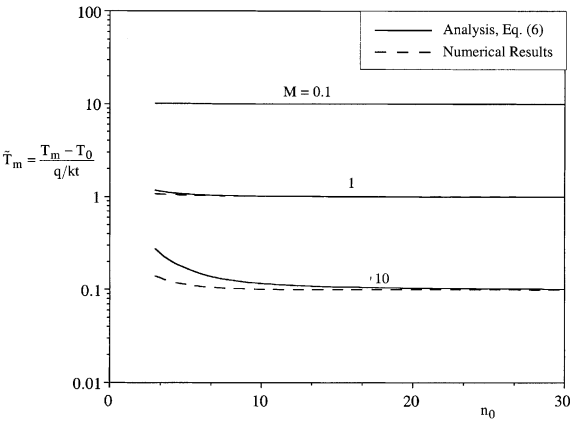


Fig. 3. The thermal resistance of the radial flow structure shown in Fig. 2: comparison between the numerical and analytical results.

decreases as $n_0$ increases, i.e., as the flow structure becomes more complex. This second trend—the effect of flow architecture—is the direction explored in the remainder of this paper.

We used the preceding analysis and the radial pattern of Fig. 2 for the purpose of developing and testing (benchmarking) the numerical simulation of heat flow in the disc-shaped system. Heat conduction was simulated numerically in a single sector, which has uniform heat generation, and a line-thin stream of coolant on the centerline. The boundaries of the sector are insulated. The equation for steady two-dimensional heat conduction in polar coordinates $(r, \theta)$ is

$$\frac{1}{\tilde{r}}\frac{\partial}{\partial\tilde{r}}\left(\tilde{r}\frac{\partial\tilde{T}}{\partial\tilde{r}}\right) + \left(\frac{n_0/\pi}{\tilde{r}}\right)^2\frac{\partial^2\tilde{T}}{\partial\tilde{\theta}^2} + \frac{1}{\pi} = 0 \tag{8}$$

where

$$\tilde{r} = \frac{r}{R} \quad \tilde{\theta} = \frac{\theta}{\pi/n_0} \quad \tilde{T} = \frac{T - T_0}{q/kt} \tag{9}$$

The boundary conditions are $\partial\tilde{T}/\partial\tilde{r} = 0$ at $\tilde{r} = 1$, $\partial\tilde{T}/\partial\tilde{\theta} = 0$ at $\tilde{\theta} = 1$, $\tilde{T} = 0$ and $\partial\tilde{T}/\partial\tilde{r} = 0$ at $\tilde{r} = 0$, and $\tilde{T}_f = (T_f - T_0)/(q/kt) = M^{-1}$ at $\tilde{r} = 1$, $\tilde{\theta} = 0$. The continuity of heat flux through the pipe wall ($\tilde{\theta} = 0$) requires

$$\frac{1}{2}M\frac{\partial\tilde{T}}{\partial\tilde{r}} = \frac{n_0^2}{\pi\tilde{r}}\frac{\partial\tilde{T}}{\partial\tilde{\theta}} \tag{10}$$

Eq. (8) was solved by the second-order accurate finite differences method. The grid was nonuniform. The grid fineness was increased in steps by decreasing the grid spacings to half of their original values, until the step change in the peak $\tilde{T}$ value [$\tilde{T}_m$, Eq. (5)] was less than 1%. The highest temperature occurred at $\tilde{r} = 1$ and $\tilde{\theta} = 1$, in accordance with the $T_m$ location indicated in Fig. 2.

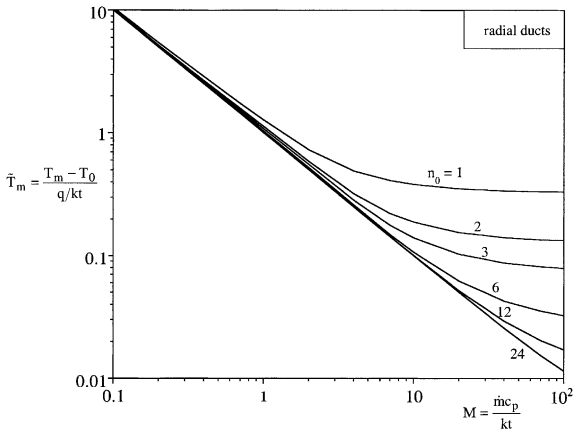


Fig. 4. Numerical solution for the thermal resistance of the radial design of Fig. 2.

Fig. 3 shows that the numerical results agree with Eq. (6) in the limit where the analysis is valid: slender sectors (large $n_0$). The numerical method was used in the remainder of the study because it does not require the use of the slender-sectors approximation. To start with, in Fig. 4 the numerical analysis of the radial design was extended to the extreme cases $n_0 = 2$ and $n_0 = 1$, which are far from the domain of applicability of Eq. (6). The overall thermal resistance decreases monotonically as $n_0$ increases, however, when $n_0$ becomes greater than approximately 6 the resistance is relatively insensitive to further increases in $n_0$.

## 3. Competition between thermal and fluid flow resistances

The radial design of Fig. 2 provides the first concrete example of the competition between the overall thermal resistance and the required overall fluid flow resistance. To show this analytically, assume that each radial duct is a round tube of diameter $D$ with Hagen-Poiseuille flow. This is the same $D$ that in Eq. (1) was the thickness of the duct image projected on the disc area. The round tube assumption is made for the purpose of illustration, because any other duct cross-section with a hydraulic diameter comparable to $D$ has fluid flow characteristics similar to those described in this section.

To evaluate the overall flow resistance encountered by the total stream $\dot{m}$, we begin with the mean fluid velocity through one tube,

$$U_0 = \frac{D^2}{32\mu}\frac{\Delta P}{R} \tag{11}$$

where $\Delta P$ is the overall pressure difference measured between the center and the periphery of the disc. The flow rate through one tube is $\dot{m}_0 = U_0\rho\pi D^2/4$. Combining $U_0$ with Eq. (11) and $\dot{m}_0 = \dot{m}/n_0$, where $\dot{m}$ is the total flow rate for the disc, we obtain the overall flow resistance

$$\frac{\Delta P}{\dot{m}} = \frac{128\nu R}{\pi n_0 D^4} \tag{12}$$

The flow resistance decreases rapidly as the duct diameter increases. This trend is resisted by requirements such as Eq. (1): the fluid flow network can occupy only a small fraction of the space occupied by the system. Assume that the total volume occupied by the ducts is fixed,

$$V = n_0\frac{\pi D^2}{4}R \tag{13}$$

so that $D$ varies as $n_0^{-1/2}$. The pumping power required by the entire assembly is $\dot{W} = \dot{m}\Delta P/\rho$. This can be expressed in dimensionless form by using Eqs. (7) and (12),

$$\widetilde{W} = 8\pi n_0 M^2 \tag{14}$$

where

$$\widetilde{W} = \dot{W}\frac{\rho c_p^2 V^2}{\nu k^2 t^2 R^3} \tag{15}$$

It can be shown that the general form of Eq. (14) is

$$\widetilde{W} = 8\pi f M^2 \tag{16}$$

where $f$ is a dimensionless flow resistance defined by

$$f = n_0\left[\sum_{j=0}^{p} 2^{j/3}\frac{L_j}{R}\right]^3 \tag{17}$$

Here $p$ is the construct level, and $L_j$ is the pipe length at the pairing level $j$. In the case of radial tubes without ramifications (Fig. 2), the factor $f$ is equal to $n_0$.

In conclusion, Eq. (14) shows that the pumping power increases in proportion to $n_0$. A small number of tubes is desirable from the fluid mechanics point of view. This message is in conflict with that of Fig. 4, which showed that a larger $n_0$ is better from the heat transfer point of view. The designer prefers low $\widetilde{W}$ and low $\widetilde{T}_m$ *at the same time*. This is why in Fig. 5 we show the result of combining Fig. 4 with Eq. (14): $M$ is the parameter that varies along each of the curves.

Which radial design ($n_0$) is best depends on the application. If the available pumping power is in the range $10^4 < \widetilde{W} < 10^5$, then the best performance (the minimal $\widetilde{T}_m$) is offered by the $n_0 = 6$ design. The optimal number of radial tubes increases as $\widetilde{W}$ increases. The ability to vary $n_0$, or the freedom to contemplate an entire family of radial designs, is represented by the "envelope" of the curves shown in Fig. 5, which is approximately $\widetilde{T}_m \cong 3.75\widetilde{W}^{-0.37}$. How this relation brings the performance in the desirable operating domain (cf. Fig. 1) is discussed in Fig. 14. This relation is not a true envelope because in Fig. 5 there is not an infinity of constant–$n_0$

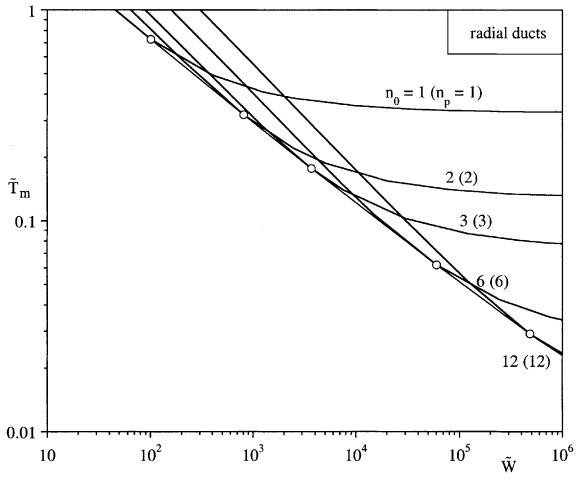


Fig. 5. The competition between overall thermal resistance and pumping power in the radial flow structure of Fig. 2.

curves. What we have is a power-law expression that plays adequately the role of common tangent for the few constant–$n_0$ curves. The points of tangency are identified with circles. They are noted (recorded and reproduced in Fig. 14) as indicators of how closely each curve approaches the desirable limit (low $\widetilde{T}_{\mathrm{m}}$, low $\widetilde{W}$). The number $n_{\mathrm{p}}$ represents the number of outlets on the disc perimeter, namely $n_{\mathrm{p}} = n_0$ in the case of radial ducts.

## 4. One level of branching: the minimization of flow resistance

One conclusion that stems from Fig. 5 is that the simplest flow structure is the best when two objectives must be met at the same time (low $\widetilde{T}_{\mathrm{m}}$ and low $\widetilde{W}$). This is true provided that the competing designs are of the same class (e.g., radial structures, Fig. 2). In this section and the next we show that there exist flow structures that are represented by curves lower than those shown in Fig. 5. They belong to classes of flow structures that are more complex than the radial designs examined until now. The more complex structures are dendritic.

Fig. 6 shows the main features of the dendritic flow structure when a single level of pairing is placed at the radial distance $L_0$. There are $n_0 = 3$ radial tubes connected to the center, and $n_{\mathrm{p}} = 2n_0$ equidistant outlets on the disc perimeter. The design has three degrees of freedom: $n_0$, $L_0$ and the ratio of the diameters of the $L_0$ and $L_1$ tubes. The optimal diameter ratio subject to total tube volume is $2^{1/3}$ [1,24]. In addition to this optimization, the dimensionless flow resistance $f$ can be minimized with respect to $L_0$ subject to the constraint of total tube volume and fixed disc radius. The total tube volume $V$ is the same as for the radial designs discussed earlier; in the present case, $V = n_0(\pi/4)D_0^2(L_0 + 2^{1/3}L_1)$. The

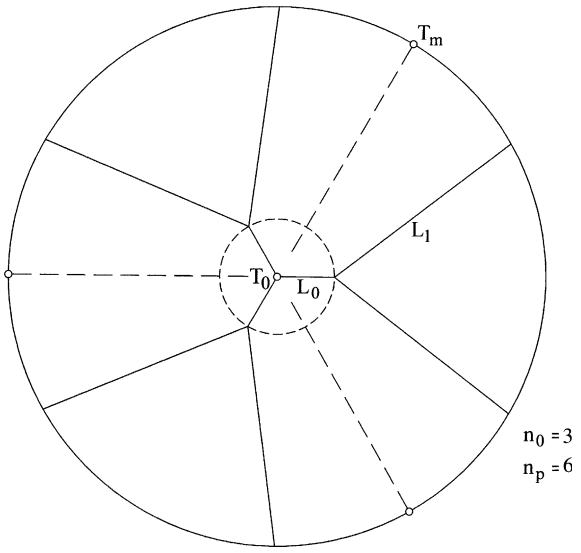


Fig. 6. The structure with $n_0 = 3$, one level of pairing and minimal flow resistance.

Table 1
Optimized flow structures with one level of pairing and minimal flow resistance (e.g., Fig. 6)

| $n_0$ | $\widehat{L}_0$ | $\widehat{L}_1$ | $f_{\min}$ |
|---|---|---|---|
| 3 | 0.214 | 0.822 | 5.849 |
| 6 | 0.628 | 0.426 | 9.471 |
| 12 | 0.821 | 0.216 | 15.605 |
| 24 | 0.913 | 0.108 | 27.625 |

optimal dimensions $(\widehat{L}_0, \widehat{L}_1)$ and performance ($f_{\min}$) are reported in Table 1, where the dimensionless lengths are

$$(\widehat{L}_0, \widehat{L}_1) = \frac{(L_0, L_1)}{R} \tag{18}$$

The drawing shown in Fig. 6 is for the case $n_0 = 3$ of Table 1, and represents an architecture optimized for minimal flow resistance.

Next, we turn our attention to the thermal performance of the structures optimized for minimal flow resistance, Table 1. The global thermal resistance of such structures was calculated and reported in Fig. 7. The behavior is qualitatively the same as what we saw in Fig. 4 for radial designs, where $\widetilde{T}_{\mathrm{m}}$ and $M$ continue to be defined as in Eqs. (5) and (7).

The pumping power that corresponds to the optimal designs of Table 1 is reported in Fig. 8, where $\widetilde{W}$ is defined as in Eq. (15). The relationship between thermal performance ($\widetilde{T}_{\mathrm{m}}$), fluid mechanics performance ($\widetilde{W}$) and complexity ($n_0$) is similar to what we found for radial designs (Fig. 5). The common tangent of the constant–$n_0$ curves in Fig. 8 is approximately $\widetilde{T}_{\mathrm{m}} \cong 5.94\widetilde{W}^{-0.4}$, which is different than the tangent found in Fig. 5. The points

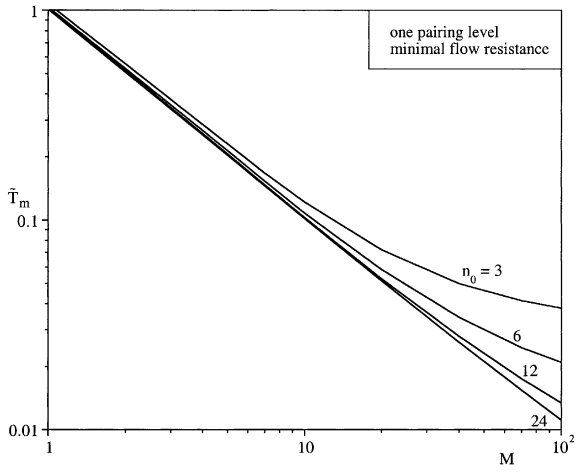


Fig. 7. The thermal resistance of structures with one level of pairing and minimal flow resistance (Table 1).

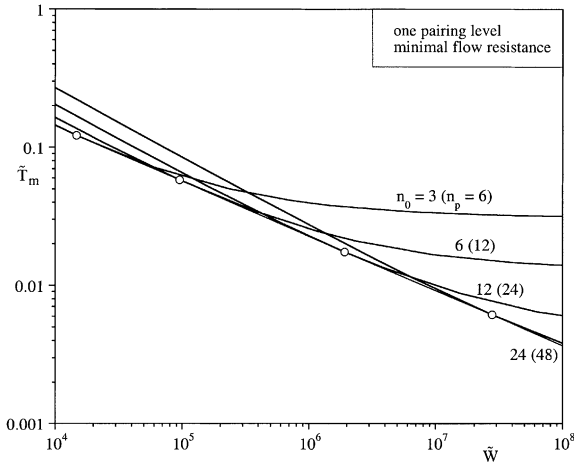


Fig. 8. The competition between overall thermal resistance and pumping power in structures with one level of pairing and minimal flow resistance (Table 1).

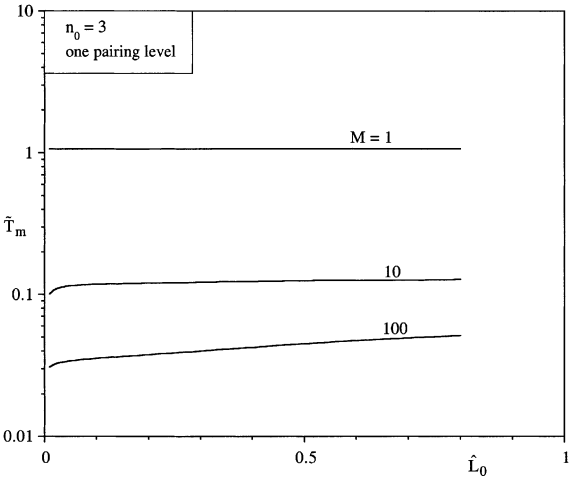


Fig. 9. The effect of the length of the innermost radial pipes ($\widehat{L}_0$) on the thermal resistance of structures with one level of pairing and $n_0 = 3$.

of tangency are identified with circles, and are reproduced in Fig. 14. Recall that in dendritic structures with one level of pairing the number of outlets on the perimeter is twice the number of central ducts, $n_p = 2n_0$.

## 5. One level of branching: the minimization of thermal resistance

The alternative to minimizing flow resistance is to minimize the thermal resistance of the structure with one level of pairing. The degrees of freedom are $n_0$ and $\widehat{L}_0$, while the flow rate number $M$ is a specified parameter. Fig. 9 shows the behavior of $\widetilde{T}_m$ when $n_0 = 3$. We found numerically that the best designs—the lowest $\widetilde{T}_m$ values—are found in the limit $\widehat{L}_0 \to 0$. In other words, from the point of view of minimizing the thermal resistance, the design with $2n_0$ radial tubes is better than any of the designs with paired tubes.

In conclusion, the thermal performance of the $\widehat{L}_0 = 0$ designs recommended by Fig. 9 is the same as what is reported in Fig. 4 for radial designs, provided that the $n_0$ values of Fig. 4 are replaced by $n_0/2$. For the same reason, the combined thermal resistance and pumping power performance is the same as in Fig. 5, provided that in Fig. 5 we put $n_0/2$ in place of $n_0$. With this substitution in mind, the common tangent of the $\widetilde{T}_m(\widetilde{W})$ curves for the $\widehat{L}_0$ designs of Fig. 9 is the same as in Fig. 5, namely $\widetilde{T}_m = 3.75\widetilde{W}^{-0.37}$. Or, if we think in terms of the number of outlets on the perimeter ($n_p$) instead of $n_0$, the common tangent found in Fig. 5 can be extended safely to the right, toward larger $\widetilde{W}$ and $n_p$ values.

## 6. Two levels of branching or pairing

The next step toward flow structures with greater complexity is shown in Fig. 10. The dendritic structure has two levels of pairing and two constraints, the total tube volume and the disc radius. The optimal ratios of successive tube diameters continue to be equal to $2^{1/3}$ [1,24]. The remaining degrees of freedom of the flow architecture are $n_0$, $\widehat{L}_0$ and $\widehat{L}_1$. The overall flow resistance $f$ has been minimized with respect to $\widehat{L}_0$ and $\widehat{L}_1$. Table 2 shows a sample of the numerical results. The $n_0 = 3$ design of Table 2 has been drawn to scale in Fig. 10.

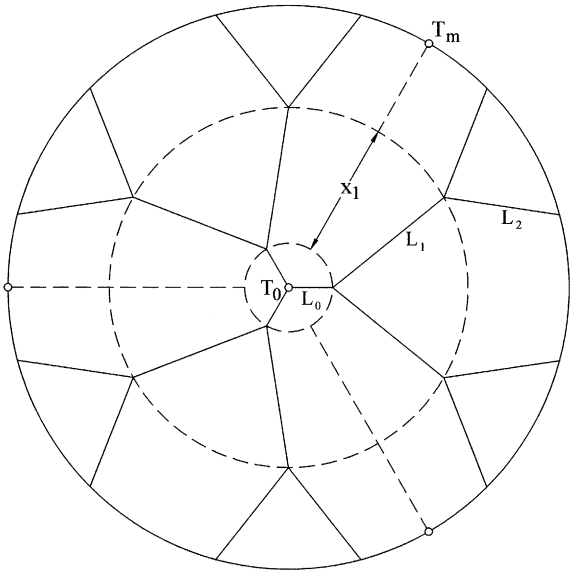


Fig. 10. Structure with two levels of pairing and minimal flow resistance ($n_0 = 3$).

Table 2
Optimized flow structures with two levels of pairing and minimal flow resistance (e.g., Fig. 10)

| $n_0$ | $\widehat{L}_0$ | $\widehat{L}_1$ | $\widehat{L}_2$ | $f_{\min}$ |
|---|---|---|---|---|
| 3 | 0.157 | 0.509 | 0.432 | 9.82 |
| 6 | 0.543 | 0.358 | 0.192 | 13.16 |
| 12 | 0.770 | 0.200 | 0.090 | 18.98 |

The overall thermal resistance that corresponds to the flow optimized designs of Table 2 is reported in Fig. 11.

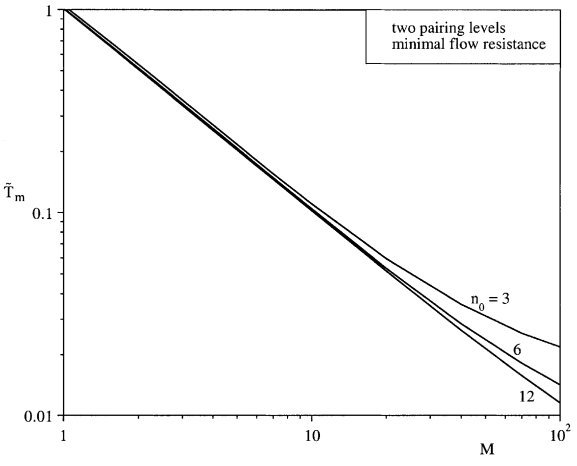


Fig. 11. The thermal resistance of structures with two levels of pairing and minimal flow resistance (Table 2).

Finally, the minimized pumping power that corresponds to these designs is reported on the abscissa of Fig. 12. The common tangent of the three curves is $\widetilde{T}_m = 8.5\widetilde{W}^{-0.43}$.

We also examined the alternative, which is to minimize the overall thermal resistance ($\widetilde{T}_m$), instead of the overall resistance to fluid flow ($f$, or $\widetilde{W}$). The degrees of freedom of the flow geometry are $n_0$, $\widehat{L}_0$ and $\widehat{L}_1$ (or $\hat{x}_1$), where ($\hat{x}_1 = x_1/R$) is the radial distance between the two levels of pairing (i.e., between the two dashed circles in Fig. 10). Fig. 13 shows the behavior of the overall thermal resistance when $\widehat{L}_0$ and $\hat{x}_1$ vary subject to constant $n_0$ and $M$. Although there is an optimal $\hat{x}_1$ when $\widehat{L}_0$ is greater than 0.2, it is clear that the lowest thermal

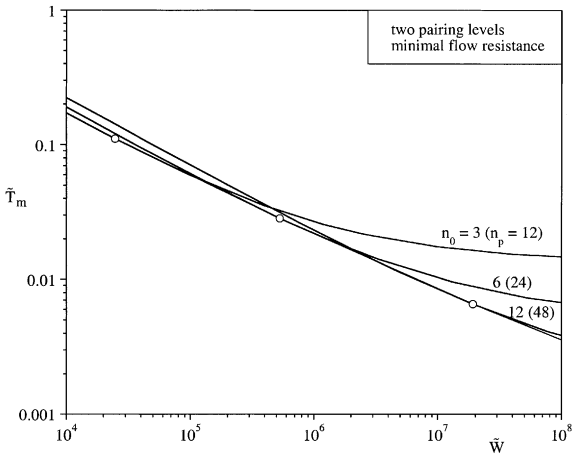


Fig. 12. The competition between overall thermal resistance and pumping power in structures with two levels of pairing and minimal flow resistance (Table 2).

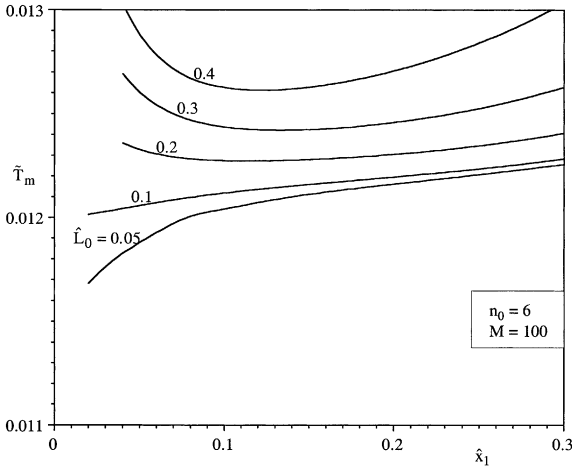


Fig. 13. The effect of the innermost length ($\widehat{L}_0$) and the radial distance between the two pairing levels ($\hat{x}_1$) on the thermal resistance of structures with two levels of pairing (e.g., Fig. 10).

resistance belongs to designs characterized by $(\widehat{L}_0, \hat{x}_1) \to 0$. These are radial designs, and their performance is again covered by Figs. 4 and 5, provided that for the present case the $n_0$ values of Figs. 4 and 5 are replaced by $n_0/4$, where $n_0$ is the number of central tubes in Fig. 10 and Table 2. The common tangent of the curves for the present designs ($\widehat{L}_0 \to 0, \hat{x}_1 \to 0$) is the same as in Fig. 5, namely $\widetilde{T}_m = 3.75\widetilde{W}^{-0.37}$.

## 7. Conclusions

Fig. 14 is a concise summary of the two classes of flow architectures that were optimized in this paper: architectures with minimal flow resistance (or minimal pumping power) vs. architectures with minimal global thermal resistance. The number of levels of branching (pairing) makes a difference when the flow geometry is selected based on the minimization of flow resistance or pumping power. When the objective is minimal global thermal resistance, the best flow pattern consists of radial ducts, and the number of pairing levels loses its effect.

An approximate reading of Fig. 14 justifies the conclusion that optimized flow structures that are complex are also robust. An optimized complex structure performs nearly as well as the next (stepwise more complex) structure. This characteristic of complex flow structures has been encountered in the design of other dendritic flows, for example, in trees for pure heat conduction and pure fluid flow [1].

A more careful reading of Fig. 14, however, leads to a conclusion of great importance in the quest for convective flow structures at smaller and smaller scales. Miniaturization and greater heat generation densities mean lower $\widetilde{T}_m$ values and higher $\widetilde{W}$ values. We see that in this direction the complexity of the flow structure and the optimization objective matter. In this limit, the ideal

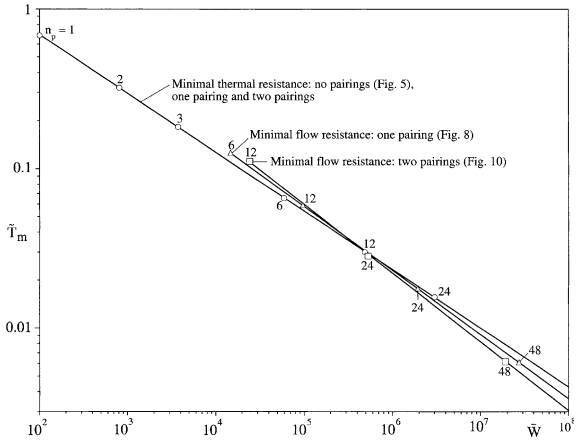


Fig. 14. The common tangents of the $\widetilde{T}_m(\widetilde{W})$ curves for the flow architectures optimized in this paper: minimal flow resistance vs. minimal thermal resistance.

expressed in Fig. 1 (low $\widetilde{T}_m$, low $\widetilde{W}$) can be achieved by using dendritic structures with increasing and optimized complexity (i.e., with more levels of pairing) and by optimizing the structure for minimal flow resistance.

Another important conclusion is that optimized complexity is a good idea only below a certain $\widetilde{T}_m$, i.e., above a certain level of miniaturization, or above a certain level of volumetric heat transfer density. The world of competing flow architectures is characterized by a sharp "transition" between the simplest structure (radial), and progressively more complex structures (dendritic). The simplest structures are preferable when $\widetilde{T}_m \gtrsim 0.03$, or $\widetilde{W} \lesssim 5 \times 10^5$. The more complex structures prevail in this competition when $\widetilde{T}_m \lesssim 0.03$, or $\widetilde{W} \gtrsim 5 \times 10^5$. Such a stepwise change in flow configuration reminds us of natural occurrences of the quest for global performance, for example, the eddy formation in fluid low (e.g., shear layers, Bénard convection) and the sudden appearance (and disappearance) of morphological changes in natural flow systems, animate or inanimate (e.g., the sudden appearance of thicker links in the time-dependent development of a river basin, while rain falls steadily on an erodable medium [1]). Similar to animal design is also the pursuit of more than one objective at the same time, in the present case, minimal flow resistance and minimal thermal resistance.

In closing, consider the engineering problem of how to select the flow pattern when the disc size ($R$) and the smallest length scale ($d_0$) are specified. These scales fix the number of outlets, $n_p$. For example, if $n_p = 24$ we may choose between the designs represented by three points in Fig. 14. The design with the smallest thermal resistance requires the largest pumping power. How to select one design out of the three possibilities depends on other considerations, such as the available pumping power. In any case, as $n_p$ increases the thermal resistance becomes insensitive to the increasing complexity, while the competing designs perform better and better hydrodynamically. In conclusion, in the limit of decreasing length scales and increasing complexity the dendritic architectures are preferable.

An alternative engineering point of view is to recognize the distance between two outlets as the smallest length scale ($d_0$, Fig. 1) of the design, and to regard it as a manufacturing constraint. This distance is held fixed. The disc radius $R$ and area $A$ increase as the number of outlets increases. Fig. 15 shows several designs for $n_p = 3$, 6 and 12, where the dendritic patterns have been optimized for minimal fluid flow resistance.

The fluid-flow performance of the hydrodynamically optimized designs with fixed $d_0$ is presented in Fig. 16. The overall pressure drop from the disc center to the periphery ($\Delta P$) is nondimensionalized as

$$\widehat{P} = \frac{V^2 \Delta P}{\dot{m}'' \nu d_0^5} \tag{19}$$

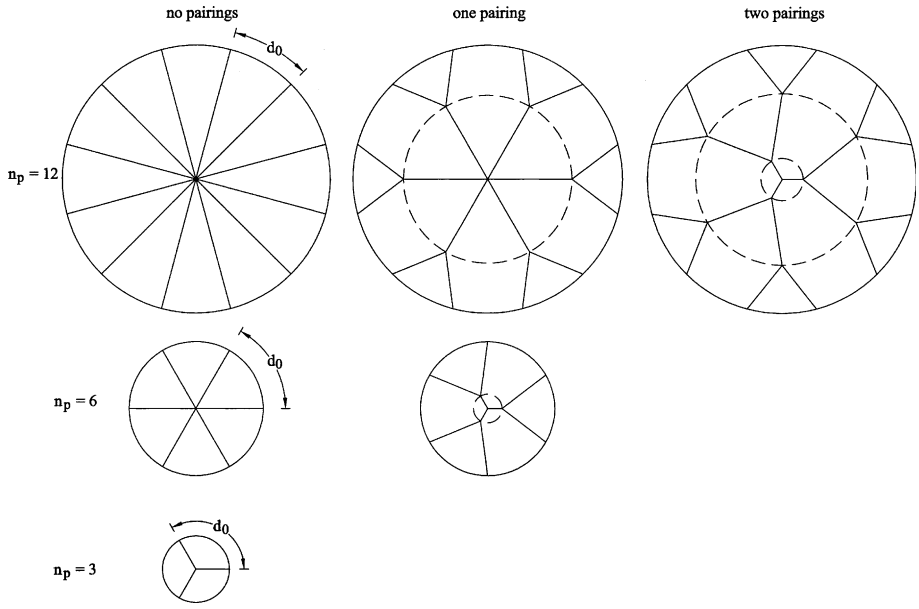


Fig. 15. Examples of hydrodynamically optimized flow structures with the same smallest scale ($d_0$) and increasing size ($n_p$, or $R$).

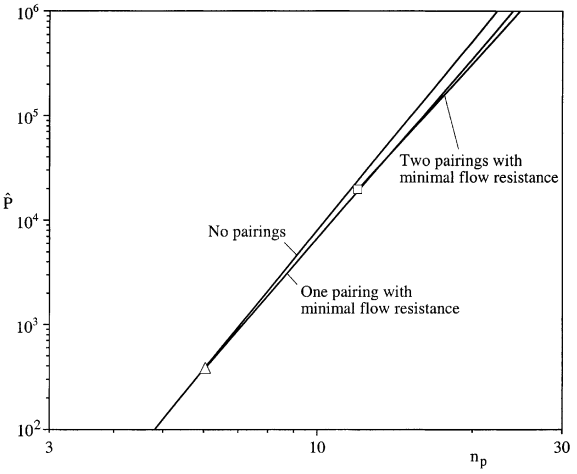


Fig. 16. The minimized overall flow resistance of structures with the same smallest scale ($d_0$) and increasing size ($n_p$, or $R$).

where the mass flow rate per unit disc area $[\dot{m}'' = \dot{m}/(\pi R^2)]$ is assumed independent of the disc radius. It can be shown that for Hagen-Poiseuille flow and optimized ratios of successive tube diameters (Section 4) the dimensionless pressure drop is

$$\widehat{P} = \frac{n_p^5 f}{4\pi^3} \tag{20}$$

for which the optimization of the flow architecture yields the minimized $f$ values (e.g., Table 1). In particular, the radial design has $f = n_p$, which means that $\widehat{P} = n_p^6/(4\pi^3)$.

Fig. 16 shows that the global flow resistance $\widehat{P}$ increases with $n_p$, i.e., with the size of the flow system. This increase, however, can be slowed down through the use of progressively more complex dendritic structures. The small circles plotted in Fig. 16 represent the starting $n_p$ values of the indicated structure. Dendrites with one level of pairing start with $n_p = 6$, while dendrites with two levels of pairing start with $n_p = 12$.

A qualitatively similar picture emerges if, instead of $\widehat{P}$ on the ordinate, we plot the dimensionless pumping power required by the design. In conclusion, we see that *optimized* complexity can be beneficial, and that the best flow structure becomes more complex as the flow system becomes larger.

## Acknowledgements

This work was supported by grants from the National Science Foundation and King Mongkut's University of Technology Thonburi (KMUTT), Thailand.

## References

[1] A. Bejan, Shape and Structure, from Engineering to Nature, Cambridge University Press, Cambridge, UK, 2000.
[2] A. Bejan, Constructal-theory network of conducting paths for cooling a heat generating volume, Int. J. Heat Mass Transfer 40 (1997) 799–816.
[3] A. Bejan, M.R. Errera, Convective trees of fluid channels for volumetric cooling, Int. J. Heat Mass Transfer 43 (2000) 3105–3118.

[4] A. Bejan, L.A.O. Rocha, S. Lorente, Thermodynamic optimization of geometry: T- and Y-shaped constructs of fluid streams, Int. J. Thermal Sci. 30 (2000) 949–960.
[5] D.V. Pence, Improved thermal efficiency and temperature uniformity using fractal-like branching channel networks, in: G.P. Celata, V.P. Carey, M. Groll, I. Tanasawa, G. Zummo (Eds.), Heat Transfer and Transport Phenomena, Begell House, New York, 2000, pp. 142–148.
[6] W. Wechsatol, S. Lorente, A. Bejan, Tree-shaped insulated designs for the uniform distribution of hot water over an area, Int. J. Heat Mass Transfer 44 (2001) 3111–3123.
[7] W. Wechsatol, S. Lorente, A. Bejan, Development of tree-shaped flows by adding new users to existing networks of hot water pipes, Int. J. Heat Mass Transfer 45 (2002) 723–733.
[8] W. Wechsatol, S. Lorente, A. Bejan, Optimal tree-shaped networks for fluid flow in a disc-shaped body, Int. J. Heat Mass Transfer 45 (2002) 4911–4924.
[9] Y. Chen, P. Cheng, Heat transfer and pressure drop in fractal tree-like microchannel nets, Int. J. Heat Mass Transfer 45 (2002) 2643–2648.
[10] S. Lorente, W. Wechsatol, A. Bejan, Tree-shaped flow structures designed by minimizing path lengths, Int. J. Heat Mass Transfer 45 (2002) 3299–3312.
[11] L.A.O. Rocha, S. Lorente, A. Bejan, Constructal design for cooling a disc-shaped area by conduction, Int. J. Heat Mass Transfer 45 (2002) 1643–1652.
[12] Z.-Z. Xia, Z.-X. Li, Z.-Y. Guo, Heat conduction optimization: high conductivity constructs based on the principle of biological evolution, Twelfth Int. Heat Transfer Conf., Grenoble, France, 18–23 August.
[13] R.A. Nelson Jr., A. Bejan, Constructal optimization of internal flow geometry in convection, J. Heat Transfer 120 (1998) 357–364.
[14] R.A. Nelson Jr., A. Bejan, Self-organization of the internal flow geometry in convective heat transfer, Proc. 7th AIAA/ASME Joint Thermophysics and Heat Transfer Conference, ASME HTD-Vol. 357-3 (1998) 149–161.
[15] L.H. Chai, M. Shoji, Self-organization and self-similarity in boiling systems, J. Heat Transfer 124 (2002) 507–515.
[16] D. Tondeur, L. Luo, U. D'Ortona, Optimisation des transferts et des materiaux par l'approche constructale, Entropie 30 (2000) 32–37.
[17] M.-O. Coppens, Y. Cheng, C.M. van den Bleek, Controlling fluidized bed operation using a novel hierarchical gas injection system, Paper 304d, AIChE Annual Meeting, Dallas, TX, October 31–November 5, 1999.
[18] A. Bejan, Dendritic constructal heat exchanger with small-scale crossflows and larger-scales counterflows, Int. J. Heat Mass Transfer 45 (2002) 4607–4620.
[19] A. Bejan, S. Lorente, Thermodynamic optimization of flow geometry in mechanical and civil engineering, J. Non-Equilibrium Thermodynamics 26 (2001) 305–354.
[20] J.E. Hesselgreaves, Compact Heat Exchangers, Pergamon, Amsterdam, 2001.
[21] S. Mahmud, R.A. Fraser, Inherent irreversibility of channel and pipe flows for non-newtonian fluids, Int. Comm. Heat Mass Transfer 29 (2002) 577–587.
[22] S. Mahmud, R.A. Fraser, Irreversibility analysis of concentrically rotating annuli, Int. Comm. Heat Mass Transfer 29 (2002) 697–706.
[23] K. Boomsma, D. Poulikakos, F. Zwick, Metal foams as compact high performance heat exchangers, Mech. Mater., in press.
[24] C.D. Murray, The physiological principle of minimal work, in the vascular system, and the cost of the blood volume, Proc. Acad. Nat. Sci. 12 (1926) 207–214.